Structural Evolution of Colloidal Crystals with Increasing Ionic Strength

Michael A. Bevan,* Jennifer A. Lewis,[†,‡] Paul V. Braun,[†] and Pierre Wiltzius[†,§]

Beckman Institute for Advanced Science and Technology, University of Illinois at Urbana-Champaign, Urbana, Illinois 61801

Received March 21, 2004. In Final Form: June 5, 2004

We have directly observed the structural evolution of colloidal crystals as a function of increasing ionic strength using confocal scanning laser microscopy. Silica colloids were sedimented onto a glass substrate in deionized water to create large, single domain crystals. The solution ionic strength was then increased by one of three methods of controlled electrolyte addition: (1) direct injection of electrolyte solutions, (2) single step diffusion of electrolyte solutions through a dialysis membrane, and (3) multiple step diffusion of electrolyte solutions of increasing ionic strength through a dialysis membrane. During direct injection of electrolyte solutions, initially large, single domain colloidal crystals were shear melted and then evolved into polycrystalline structures at low ionic strengths and gels at higher ionic strengths. Diffusion of electrolyte solutions though dialysis membranes in a single step produced gradient-driven transport that also melted initial single domain crystals to yield polycrystalline and gel structures similar to the injection approach. Interestingly, the multistep diffusion of several electrolyte solutions through dialysis membranes facilitated retention of large, single domain crystals even as particles came into adhesive contact. This was achieved by reducing the contraction rate of the crystalline lattice to allow sufficient time for diffusion-limited configurational rearrangements to occur within the evolving structure. These mechanically robust, single domain colloidal crystals may find important applications as templates for photonic materials and sensors.

Introduction

Three-dimensional microperiodic structures fabricated from colloidal "building blocks" may find widespread technological use in applications such as advanced ceramics,[1] composites,[2] sensors,[3] and templates for photonic band gap materials.[4] Aqueous colloids are known to self-assemble into large, single crystal domains at low ionic strength conditions.[5] However, these crystals are mechanically weak due to the extended electrostatic double layer surrounding each particle.[6] As a result, simple shear alone is sufficient to induce melting[7] and structural transitions.[8] Moreover, attempts to create dried, adhesive colloidal crystals from such systems are generally limited by the formation of polycrystalline domains and cracks during drying.[9]

Several methods for assembling large, single domain crystals have recently been introduced, which rely on capillary-driven consolidation (e.g., using a fluidic cell[10] or dip coating[11,12]) or colloidal epitaxy.[13] However, scant attention has been given to creating mechanically robust crystals through tuning colloidal interactions to produce adhesive particle contacts while simultaneously preserving long-range order. Our approach relies on first assembling colloidal crystals with repulsive electrostatic interactions that extend well away from the particle surfaces, followed by tuning particle interactions through controlled electrolyte addition to allow van der Waals attraction to dominate. Because the face-centered cubic (fcc) crystal structure is the lowest free energy configuration for colloids with repulsive electrostatic,[5,14,15] hard sphere,[16−18] and attractive van der Waals potentials,[19−21] in principle it should be possible to design processes for assembling single domain, fcc colloidal crystals at nearly any ionic strength. This is true provided that challenges, such as formation of kinetically trapped glassy[22−24] or irreversible gel[25,26] structures, associated with simply increasing the attraction between colloids via uncontrolled electrolyte addition can be overcome.

Several studies have probed structures, interactions, and dynamics relevant to colloidal crystal assembly using

* To whom correspondence should be addressed. E-mail: mabevan@tamu.edu. Current address: Department of Chemical Engineering, Texas A&M University, College Station, TX 77843-3122.

† Department of Material Science and Engineering.

‡ Department of Chemical and Biomolecular Engineering.

§ Department of Physics.

(1) Lewis, J. A. *J. Am. Ceram. Soc.* **2000**, *83*, 2341.
(2) Ash, B. J.; Schadler, L. S.; Siegel, R. W. *Mater. Lett.* **2002**, *55*, 83.
(3) Holtz, J. H.; Asher, S. A. *Nature* **1997**, *389*, 829.
(4) Yablonovitch, E. *Phys. Rev. Lett.* **1987**, *58*, 2059.
(5) Sirota, E. B.; Ou-Yang, H. D.; Sinha, S. K.; Chaikin, P. M. *Phys. Rev. Lett.* **1989**, *62*, 1524.
(6) Russel, W. B.; Saville, D. A.; Schowalter, W. R. *Colloidal Dispersions*; Cambridge University Press: New York, 1989.
(7) Grier, D. G.; Murray, C. A. *J. Chem. Phys.* **1994**, *100*, 9088.
(8) Ackerson, B. J.; Clark, N. A. *Phys. Rev. A* **1984**, *30*, 906.
(9) Routh, A. F.; Russel, W. B. *Langmuir* **1999**, *15*, 7762.
(10) Park, S. H.; Xia, Y. *Langmuir* **1999**, *15*, 266.
(11) Jiang, P.; Bertone, J. F.; Hwang, K. S.; Colvin, V. L. *Chem. Mater.* **1999**, *11*, 2132.
(12) Vlasov, Y. A.; Bo, X.-Z.; Sturm, J. C.; Norris, D. J. *Nature* **2001**, *414*, 289.
(13) van Blaaderen, A.; Ruel, R.; Wiltzius, P. *Nature* **1997**, *385*, 321.
(14) Kose, A.; Ozka, M.; Takano, K.; Kobayashi, Y.; Hachisu, S. *J. Colloid. Interface Sci.* **1973**, *44*, 330.
(15) Monovoukas, Y.; Gast, A. P. *Langmuir* **1991**, *7*, 460.
(16) Hachisu, S.; Kobayashi, Y. J. *J. Colloid. Interface Sci.* **1974**, *46*, 470.
(17) Ackerson, B. J.; Schatzel, K. *Phys. Rev. E* **1995**, *53*, 6448.
(18) Gasser, U.; Weeks, E. R.; Schofield, A.; Pusey, P. N.; Weitz, D. A. *Science* **2001**, *292*, 258.
(19) Smithline, S. J.; Haymet, A. D. J. *J. Chem. Phys.* **1985**, *83*, 4103.
(20) Marr, D. W.; Gast, A. P. *J. Chem. Phys.* **1993**, *99*, 2024.
(21) Kose, A.; Hachisu, S. *J. Colloid Interface Sci.* **1976**, *55*, 487.
(22) Tokuyama, M. *Phys. Rev. E* **2000**, *62*, R5915.
(23) Rosenbaum, D.; Zamora, P. C.; Zukoski, C. F. *Phys. Rev. Lett.* **1996**, *76*, 150.
(24) Dawson, K. A. *Curr. Opin. Colloid Interface Sci.* **2002**, *7*, 218.
(25) Buscall, R.; Mills, P. D. A.; Goodwin, J. W.; Lawson, D. W. *J. Chem. Soc., Faraday Trans. 1* **1988**, *84*, 4249.
(26) Lin, M. Y.; Lindsay, H. M.; Weitz, D. A.; Ball, R. C.; Klein, R.; Meakin, P. *Nature* **1989**, *339*, 360.

10.1021/la0492658 CCC: $27.50
Published on Web 07/22/2004

optical microscopy[14−16,18,21,27−30] and scattering techniques.[5,31,32] Although shear melting of colloidal crystals has previously been investigated,[7] to our knowledge, the degree of crystallinity that emerges at different ionic strengths following fluidization has not been systematically studied. We are aware of only a single investigation that has studied melting of colloidal crystals via salt addition, and in this case, the primary focus was characterization of freezing kinetics during a subsequent deionization step.[27] The majority of studies have focused only on low ionic strength conditions, thereby neglecting the structural evolution of colloidal crystals at higher ionic strengths. Recently, Bergstrom and co-workers[33] reported structures of dried colloidal crystal monolayers as a function of electrolyte concentration and evaporation rate. They observed ionic strength to have a strong effect on the structural quality of the dried films, whose characteristic domain sizes decreased exponentially with increasing salt concentration. Their observations, however, were confined solely to dried monolayer films.

Here, we report the structural evolution of large, single domain colloidal crystals as a function of controlled electrolyte addition using three different methods: (1) injection of electrolyte solutions, (2) single step diffusion of electrolyte solutions through a dialysis membrane, and (3) multistep diffusion of electrolyte solutions through a dialysis membrane. Confocal scanning laser microscopy was used to directly observe structural evolution in the bottom layer of sedimented colloidal crystals for each method of electrolyte addition. In the interpretation of our results, special attention is given to the role of diffusion-limited rearrangement processes in the formation of disordered, kinetically trapped structures (e.g., colloidal gels and glasses). Our observations reveal that it is possible to preserve the inherent long-range order associated with colloidal crystals initially assembled under low ionic strength conditions through a novel pathway of controlled electrolyte addition to ultimately yield adhesive colloidal crystals.

Experimental Section

Materials. Nominal 1 μm silica colloids (Geltech, Alachua, FL) were dispersed in double deionized (DDI) water using an ultrasonic horn followed by shaking for 24 h. After the particles were cleaned by repeated sedimentation, decantation, and redispersion, a particle size of 1.2 ± 0.02 μm was consistently measured using scanning electron microscopy, confocal scanning laser microscopy, and dynamic light scattering. Their density of 2.25 g/cm^3 was determined by helium pycnometry (model AccuPyc 1330, Micrometrics Instrument Corp., Norcross, GA). No ion-exchange resins were employed in this study; therefore, the initial ionic strength of the aqueous medium was expected to be ~10^{-5} M at a solution pH of 5.5. The particle zeta potential was measured to be approximately −60 mV under these conditions, and its isoelectric point was determined to be at a pH of ~2.5 from electrophoretic mobility measurements (ZetaSizer 3000 HSa, Malvern Instruments, Southborough, Boston, MA). The sodium chloride (NaCl) used to control ionic strength in these experiments was purchased from Aldrich and used without further purification.

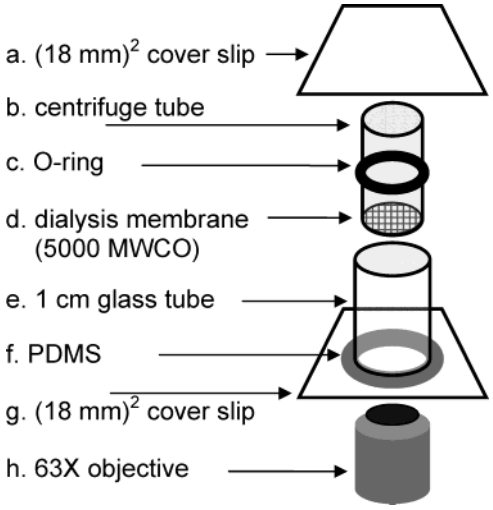

Figure 1. Schematic of the sedimentation cell and dialysis membrane: (a) 18 mm × 18 mm × 6170 μm coverslip, (b−d) centrifuge tube with a 5 kDa NMWCO dialysis membrane supported by an O-ring, (e−g) 1.2 cm o.d. × 1.0 cm i.d. × 1 cm high glass tube attached to the coverslip with PDMS, (h) 63× objective.

Colloidal Crystal Assembly. Colloidal crystals were assembled in sedimentation cells shown schematically in Figure 1. Each cell was constructed by attaching 1 cm × 1.2 cm × 1 cm (i.d. × o.d. × h) glass tubes to 18 mm × 18 mm × 170 μm (l × w × d) cover glasses (Corning) using polydimethyl siloxane (PDMS, Sylgard 184, Dow Corning). To maximize the negative surface potential on the silica coverslip surface,[34] sedimentation cells were soaked in piranha solution (3 parts concentrated H_2SO_4/1 part 30% H_2O_2 in water) and 0.1 M NaOH each for 24 h and then stored in DDI water. Prior to their use, the cells were rinsed with DDI water and dried with nitrogen. Tubes containing 5 kDa nominal molecular weight cutoff (NMWCO) dialysis membranes (Millipore Biomax filtration centrifuge tubes) were inserted into sedimentation cells and held in place by O-rings as shown in Figure 1. The bottom of the dialysis tube was placed ~1 mm above the top of ~1 mm thick sedimented colloidal crystals.

Colloidal dispersions were introduced into sedimentation cells by mixing 400 μL of DDI water with 100 μL of 20% (v/v) dispersed 1.2 μm silica colloids. Samples were allowed to sediment for 16 h during which tubes were covered with 18 mm × 18 mm × 170 μm (l × w × d) coverslips to minimize evaporation. At the beginning of each experiment, sedimentation cells were placed on the microscope stage and left undisturbed for 15 min, at which point the particle motion was indistinguishable from that of samples left undisturbed for 24 h. Sedimentation cells were ensured to be normal to gravity using a three-point leveling stage. For "injection" experiments, electrolyte was pipetted directly into the supernatant solution above the sedimented crystal. For "diffusion" experiments, electrolyte was pipetted into the dialysis tube and allowed to diffuse through a 5 kDa NMWCO membrane into the supernatant solution above the sedimented colloids. Dialysis tubes were prewet with deionized water in a centrifuge to avoid trapping air in the membrane, which affects transport rates if left uncontrolled. In each experiment, 500 μL of electrolyte solution with an ionic strength twice the desired final ionic strength was added to the dialysis tube.

Confocal Imaging of Structural Evolution. A Leica SP2 confocal scanning laser microscope (CSLM) was used to image the first layer of sedimented colloidal crystals adjacent to the coverslip substrate surface immediately (<1 s) after electrolyte addition. The CSLM was operated in reflection mode using a 633 nm wavelength helium−neon laser. In each experiment, a 63× objective with a numerical aperture (NA) of 1.4 was used with a zoom of 4, which corresponds to a 59.524 μm × 59.524 μm image. At the beginning and end of kinetic experiments, a single

(27) Yoshida, H.; Ito, K.; Ise, N. *Phys. Rev. B* **1991**, *44*, 435.
(28) van Blaaderen, A.; Wiltzius, P. *Science* **1995**, *270*, 1177.
(29) Dinsmore, A. D.; Weeks, E. R.; Prasad, V.; Levitt, A. C.; Weitz, D. A. *Appl. Opt.* **2001**, *40*, 4152.
(30) Crocker, J. C.; Grier, D. G. *J. Colloid Interface Sci.* **1996**, *179*, 298.
(31) Hurd, A. J.; Clark, N. A.; Mockler, R. C.; O'Sullivan, W. J. *Phys. Rev. A* **1982**, *26*, 2869.
(32) Derksen, J.; Water, W. v. d. *Phys. Rev. A* **1992**, *45*, 5660.
(33) Rodner, S. C.; Wedin, P.; Bergstrom, L. *Langmuir* **2002**, *18*, 9327.
(34) Iler, R. K. *The Chemistry of Silica*; Wiley: New York, 1979.

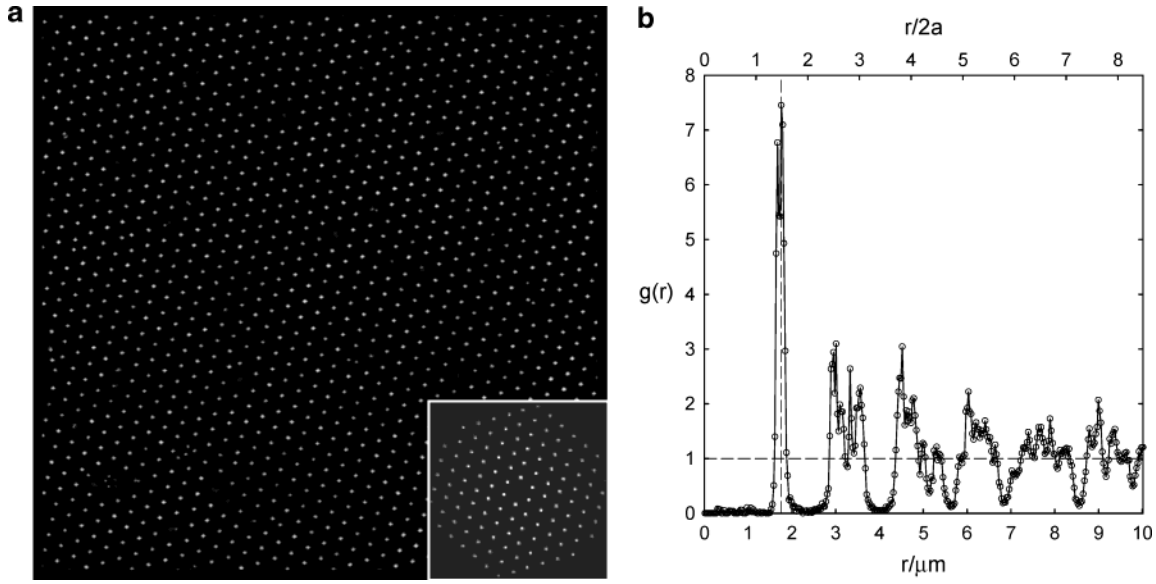

Figure 2. (a) Reflectance CSLM image and two-dimensional number density, $N(r,\theta)$ (inset), for the first layer of sedimented colloidal crystal without added electrolyte; (b) radial distribution function, $g(r)$.

2048 × 2048 resolution (pixel = 0.0291 μm) image was obtained. During kinetic experiments, 512 × 512 resolution (pixel = 0.1163 μm) images were obtained in 5 s intervals. Despite a rapid reduction in imaging capabilities as a function of height above the first layer, it was possible to generate images to a depth of ~5 particle diameters that could be analyzed using our image analysis code without modification. Except for gradually increasing noise and signal attenuation, image analysis revealed that average particle separations and bond order parameters were identical to values reported for the first layer in each experiment.

Characterization of Structural Evolution. To dynamically probe sedimented colloidal structure as a function of ionic strength, image analysis algorithms were used to locate particle centers in two-dimensional image slices parallel to the bottom coverslip surface in Figure 1. Using Fortran code developed in our group, images were processed using typical algorithms for locating particle centers from local intensity maxima.[30] Several approaches were used to quantitatively analyze the degree of order from particle center coordinates. Colloidal order in two-dimensional images can be visually evaluated by plotting the average two-dimensional number density, $N(r,\theta)$,[35]

$$N(r,\theta) = \langle \rho(n,r,\theta) \rangle_n \tag{1}$$

which is the two-dimensional density around each particle averaged over all particles (see examples in the insets of Figures 2−4 and 6). By taking the angular average of $N(r,\theta)$ and normalizing by the total average density, the radial distribution function, $g(r)$, was calculated for each image using

$$g(r) = \frac{\langle \rho(n,r,\theta) \rangle_{n,\theta}}{\langle \rho(n,r,\theta) \rangle_{n,r,\theta}} = \frac{\rho(r)}{\langle \rho \rangle} \tag{2}$$

where $\langle \rho \rangle$ is the density averaged over all particles and directions, which is simply the bulk density. A single parameter useful for characterizing two-dimensional order is a global bond orientational order parameter given as[36]

$$\psi_X = \left| \frac{1}{N} \sum_j \sum_k e^{Xi\theta_{jk}} \right| \tag{3}$$

where X is an integer related to the coherence of X-fold symmetry, that is, $X = 6$ for hexagonal 6-fold symmetry and $X = 4$ for square 4-fold symmetry. Regardless of the symmetry type, ψ_X approaches 1 for perfect order or a number approaching zero for random configurations.

(35) Loudiyi, K.; Ackerson, B. J. *Physica A* **1992**, *184*, 1.
(36) Halperin, B. I.; Nelson, D. R. *Phys. Rev. Lett.* **1978**, *41*, 121.

Results

Initial Colloidal Crystals. Large, single domain colloidal crystals were assembled in the absence of added electrolyte as shown in Figure 2a. The corresponding radial distribution function, $g(r)$, and average two-dimensional number density, $N(r,\theta)$, for a representative confocal image acquired for this sample are provided in Figure 2b. The colloidal crystal had an average interparticle surface separation ($r - 2a$) of 500 nm resulting from the low ionic strength conditions. Bond orientational order parameters for 6-fold order, $\psi_6 = 0.93$, and 4-fold order, $\psi_4 = 0.08$, were calculated from eq 3. Using the CSLM, we observed that the lateral dimensions of this single crystalline domain crystal (~0.5 cm^2 area) far exceeded the imaged region (~3.5 × 10^{-5} cm^2 area) shown in Figure 2a. Measurements at different locations in the sedimented crystal were quantitatively indistinguishable in terms of crystalline orientation, particle spacing, and bond order parameters.

Structure Evolution during Electrolyte Injection. Our first approach for altering the solution ionic strength was to directly inject electrolyte solutions of varying concentration into the large, single domain crystals such as the one in Figure 2. Confocal movies were acquired to monitor structural evolution upon injecting electrolyte solutions to produce final ionic strengths of (a) 0.1 mM, (b) 1 mM, (c) 10 mM, and (d) 1000 mM NaCl. The results for each ionic strength are presented in Figure 3 (in columns), where column i depicts kinetic data for average interparticle separation distance and ψ_6 as a function of time, column ii depicts CSLM images and two-dimensional number densities, $N(r,\theta)$, acquired at the conclusion of each assembly period, and column iii shows radial distribution functions, $g(r)$, for each corresponding image. A summary of the measured structure, two-dimensional area fraction, and ψ_6 is provided in Table 1.

The forced convection associated with injection of electrolyte solutions completely shear melted (fluidized) the large, single domain colloidal crystals into random configurations as revealed by an initial value of $\psi_6 = 0$ in each kinetic data set. In conjunction with shear melting,

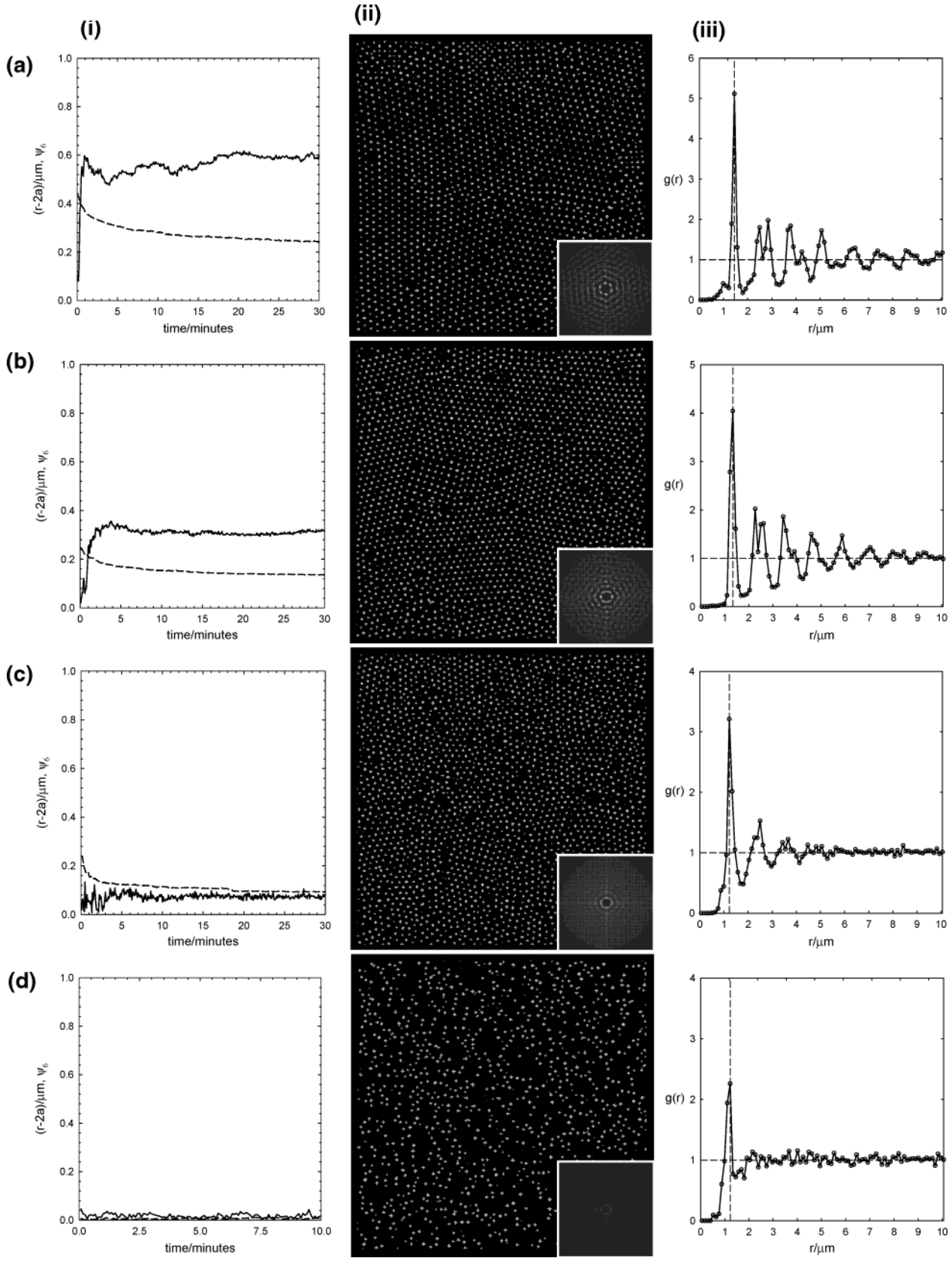

Figure 3. Structural evolution of sedimented colloidal crystals (initially assembled without added electrolyte) upon injection of (a) 0.1 mM, (b) 1 mM, (c) 10 mM, and (d) 1000 mM NaCl. Column i: particle surface separation, $r - 2a$ (dashed line), and 6-fold bond orientational order, ψ_6 (solid line), as a function of time. Column ii: reflectance image and two-dimensional number density, $N(r,\theta)$ (inset), for the first layer. Column iii: radial distribution function, $g(r)$.

the average interparticle separation ($r - 2a$) was observed to dramatically decrease on a time scale much faster than reliable confocal imaging could be commenced. Several minutes after bulk electrolyte injection, particle separation reached a plateau value consistent with the diminished range of repulsive electrostatic forces at each ionic

Table 1. Colloidal Structure as a Function of Ionic Strength and Electrolyte Addition Method

	injection			single step diffusion			multiple step diffusion		
	structure	ϕ_A	ψ_6	structure	ϕ_A	ψ_6	structure	ϕ_A	ψ_6
no added salt	crystal	0.40	0.93	crystal	0.40	0.93	crystal	0.40	0.93
0.1 mM	polycrystal	0.61	0.60	crystal			crystal		
1 mM	polycrystal	0.67	0.32	crystal	0.44	0.85	crystal	0.52	0.88
10 mM	polycrystal	0.70	0.08	polycrystal	0.52	0.85	crystal	0.61	0.84
100 mM	gel			polycrystal	0.65	0.20	crystal	0.69	0.83
1000 mM	gel	0.37	0.02	gel	0.54	0.12	crystal	0.70	0.77

strength. Values of ψ_6 plateaued on slightly faster time scales than particle separation. In control experiments (not shown in Figure 3), injecting DDI water to induce shear melting in low ionic strength crystals resulted in the re-emergence of single crystals with $\psi_6 \cong 0.90-0.95$ identical to initial colloidal crystals (see Figure 2). In these control experiments, structural evolution occurred too rapidly (<1 s) for confocal imaging.

With increasing ionic strength in each experiment in Figure 3, values of ψ_6 decreased significantly from the values of $\psi_6 \cong 0.90-0.95$ observed for initial large, single domain crystals. After shear melting, ψ_6 recovered from zero to respective plateau values of approximately 0.60, 0.32, and 0.08 for 0.1, 1, and 10 mM NaCl solutions, while remaining near zero for the 1000 mM case. Correspondingly, the characteristic domain sizes associated with the polycrystalline structures decreased from ~25 to ~5 particle diameters as the ionic strength increased from 0.1 to 10 mM NaCl. At the highest ionic strength studied (i.e., 1000 mM NaCl solution), a disordered colloidal gel formed as shown in Figure 3d. Adhesive particle contacts within the gel structure were confirmed from the average particle separation (peak at $r = 2a$ in $g(r)$) and the ability to tilt the sample without inducing flow as evidence of a macroscopic yield stress.

Structure Evolution during Single Step Electrolyte Diffusion. To suppress forced convection and associated shear melting, our second approach for increasing solution ionic strength involved diffusive transport of electrolyte solutions through a dialysis membrane supported above sedimented crystals as depicted in Figure 1. Similar to the injection experiments, confocal movies were acquired to monitor the structural evolution during diffusion of electrolyte solutions to produce final ionic strengths of (a) 1 mM, (b) 10 mM, (c) 100 mM, and (d) 1000 mM NaCl. These results are presented in Figure 4 with a format identical to that of the injection experiment results reported in Figure 3. In addition to ψ_6, kinetic data in Figure 4 report 4-fold order parameters, ψ_4, to monitor formation of square crystalline lattices and point and line defects. Table 1 summarizes structural parameters for each ionic strength condition.

The single step diffusion approach suppressed forced convection as a dominant transport mechanism, as confirmed by the initial retention of long-range order ($\psi_6 \cong 0.9$) in the kinetic results shown in Figure 4. Initial particle separations were similar to the values of ~500 nm observed for colloidal crystals assembled in the absence of added salt (see Figure 2). Following this initial period, particle separation decreased gradually in the 1 and 10 mM experiments and abruptly in the 100 and 1000 mM experiments, indicating the onset of electrolyte transport into the bottom layer of the sedimented crystals. Although particle separation did not fully re-equilibrate for the 1 and 10 mM experiments in the 30 min observation period reported in Figure 4a,b, it ultimately converged to values similar to those reported for the crystals produced via electrolyte injection at the same ionic strengths in Figure 3b,c. At higher salt concentrations, particle separation decreased rapidly to final plateau values within 5−10 min for 100 mM salt addition and 2−5 min for the 1000 mM salt addition.

In contrast to direct electrolyte injection, a significantly higher degree of 6-fold order was maintained using the single step diffusion approach. At low salt concentrations (≤10 mM NaCl), structures remained ordered as indicated by final plateau values of $\psi_6 \cong 0.80$. At a higher salt concentration of 100 mM NaCl, a polycrystalline structure formed that was comprised of both hexagonal and square domains. In this case, ψ_6 decreased to ~0.20 and ψ_4 increased to ~0.10. This result is in sharp contrast to the disordered structure observed in the 100 mM injection experiment. Finally, for the 1000 mM single step diffusion experiment, a disordered colloidal gel formed similar to the 1000 mM injection experiment (see Figure 4d) with final ψ_6 and ψ_4 values of 0.10 and 0.02.

Structure Evolution during Multistep Electrolyte Diffusion. Our final approach for increasing solution ionic strength involved the multistep diffusive transport of electrolyte solutions of increasing concentration through a dialysis membrane supported above the sedimented crystals. Using a micropipet, the ionic strength was increased in the dialysis tube reservoir at specified intervals by removing low ionic strength solutions and replacing them with higher ionic strength solutions. This approach eliminated forced convection and simultaneously reduced gradient-driven transport by minimizing ionic strength differences across the dialysis membrane at any given time during the assembly process. Figure 5 depicts particle separation distance, ψ_6, and ψ_4 as a function of time during the addition of electrolyte solutions with the following ionic strengths: (a) 1 mM for 30 min, (b) 10 mM for 15 min, (c) 100 mM for 15 min, (d) 1000 mM for 7.5 min, and finally (e) 1000 mM HCl. Figure 6 shows a CSLM image and corresponding $g(r)$ data for the final structure obtained at the completion of the 75 min electrolyte addition process in Figure 5. As summarized in Table 1, single domain ordered structures were preserved at each ionic strength and throughout the course of the experiment in Figure 5.

In the first step in Figure 5, 1 mM NaCl was equilibrated with the sedimented crystal for 30 min, which resulted in a significant decrease in particle separation and a 2−3 order of magnitude increase in ionic strength. In the next two steps, 10 and 100 mM NaCl were added in 15 min intervals during which particle separation decreased to nearly zero. In the final two steps, 1000 mM NaCl and 1000 mM HCl were added to minimize electrostatic repulsion at the silica isoelectric point,[34] which was intended to maximize the net particle attraction and yield stress in the final adhesive colloidal crystal.[37] The term "adhesive" is used here to describe colloidal crystals with particles in adhesive contact that exhibit a macroscopic yield stress, as demonstrated by the ability to tilt the sample without inducing flow. While ψ_6 fluctuated during

(37) Buscall, R.; Ettelaie, R.; Healy, T. W. *J. Chem. Soc., Faraday Trans.* **1997**, *93*, 4009.

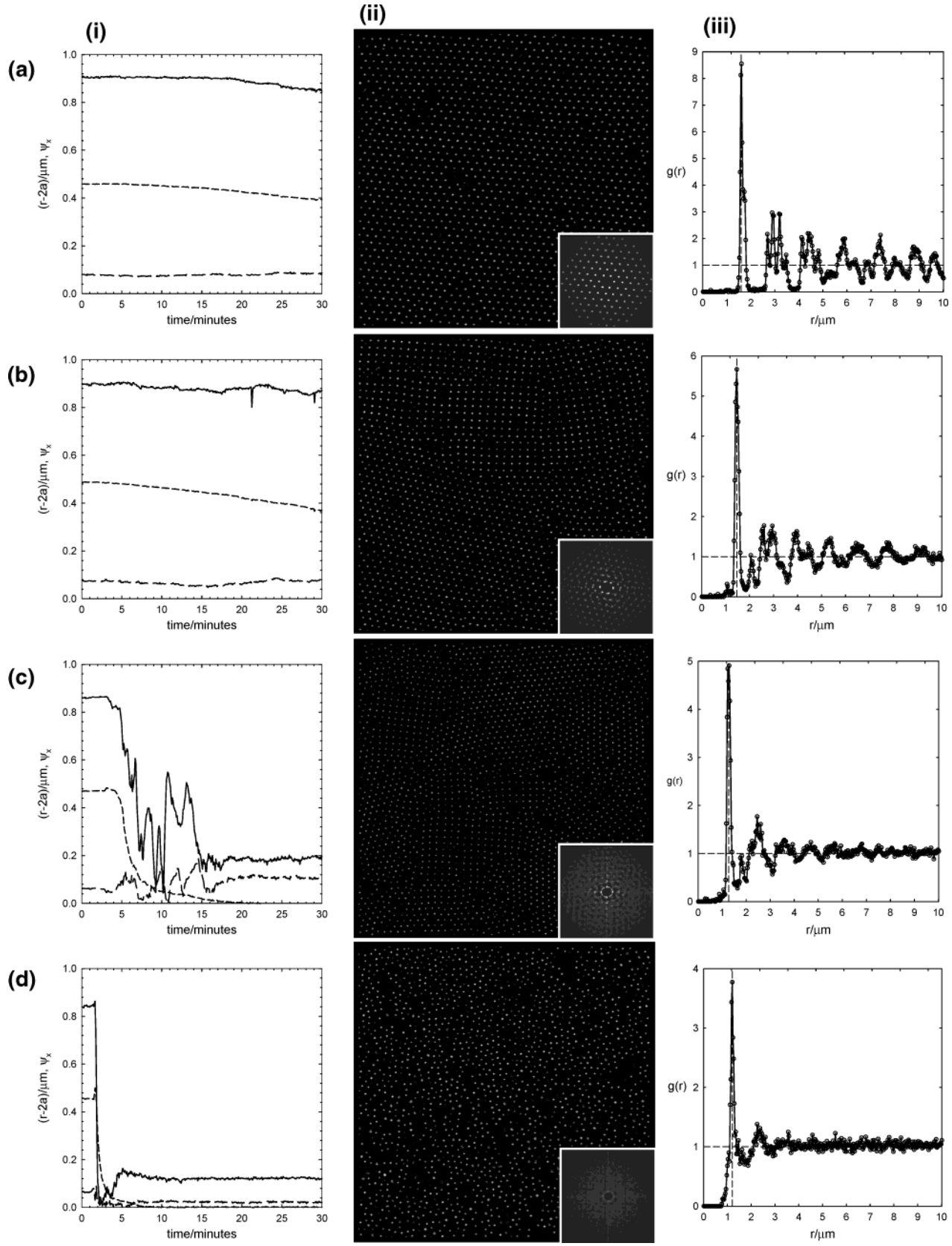

Figure 4. Structural evolution of sedimented colloidal crystals (initially assembled without added electrolyte) upon single step diffusion of (a) 0.1 mM, (b) 1 mM, (c) 10 mM, and (d) 1000 mM NaCl. Column i: particle surface separation, $r - 2a$ (short dashed line), 6-fold bond orientational order, ψ_6 (solid line), and 4-fold bond orientational order, ψ_4 (long dashed line), as a function of time. Column ii: reflectance image and two-dimensional number density $N(r,\theta)$ (inset), for the first layer. Column iii: radial distribution function, $g(r)$.

this process, a consistently high value of ~0.75 was maintained, whereas ψ_4 remained near zero. Based on direct observation, the crystallinity and macroscopic orientation were unchanged during the entire process of electrolyte addition; that is, no transient polycrystalline or square lattice domains formed. Equally important, the

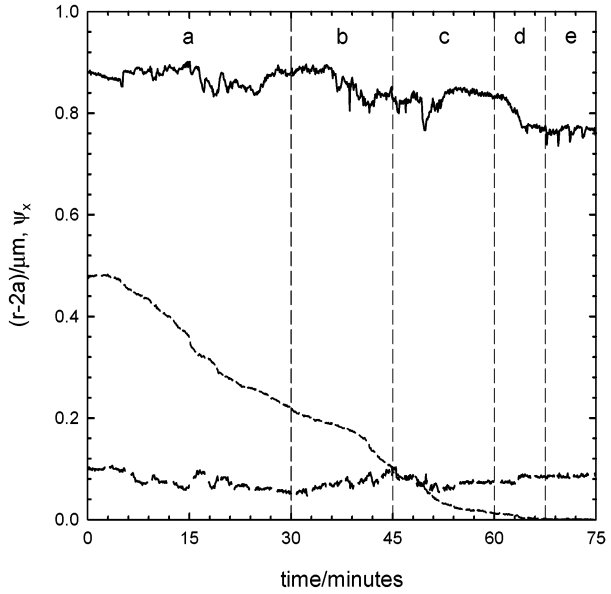

Figure 5. Structural evolution of sedimented colloidal crystals (initially assembled without added electrolyte) upon multiple step diffusion of (a) 1 mM, (b) 10 mM, (C) 100 mM, (d) 1000 mM NaCl, and (e) 1000 mM HCl where particle surface separation, $r - 2a$ (short dashed line), 6-fold bond orientational order, ψ_6 (solid line), and 4-fold bond orientational order, ψ_4 (long dashed line), are plotted as a function of time.

lateral dimensions of this single crystalline domain (~0.5 cm^2 area) far exceed the imaged region (~3.5×10^{-5} cm^2 area) shown in Figure 6, and measurements taken at different locations within the crystal were quantitatively indistinguishable in terms of crystalline orientation, particle spacing, and bond order parameters.

Discussion

Macroscopic, single domain colloidal crystals rapidly assemble under low ionic strength conditions because a large average interparticle separation allows them to freely diffuse and easily adopt their lowest free energy configuration. However, these low ionic strength colloidal crystals are extremely fragile and susceptible to shear melting that often limits their practical use. In this work, we demonstrate a new assembly route involving controlled, multistep diffusive transport of electrolyte solutions that exploits the inherent long-range order at low ionic strengths by preserving crystallinity even as colloidal particles are brought into adhesive contact. As a result, mechanically robust single domain crystals can be readily assembled following this novel approach. Here we discuss the impact of various electrolyte addition methods on structural evolution during colloidal assembly, focusing first on electrolyte injection and then on single and multistep diffusion through dialysis membranes.

Our observations can be understood in terms of a competition between two dynamic processes that control structural evolution in each assembly method investigated. One process involves structural contraction with a characteristic rate $\lambda_{contract} = (dr/dt)/a$, which is the time-dependent change in average particle separation divided by particle radius. This rate can be evaluated directly from kinetic results in Figures 3−5. The other process involves particle diffusion with a characteristic rate $\lambda_{diff} = D_s/a^2$, which is the rate of particle motion within evolving structures due to Brownian motion and hydrodynamic interactions characterized by a self-diffusion coefficient divided by particle radius squared. This rate can be estimated by computing either short- or long-time self-diffusion coefficients depending on the distances over which particles must move to rearrange.

Beginning with the injection experiments, the observed decrease in long-range order with increasing ionic strength mainly reflects the corresponding decrease in the particle diffusion rate that limits emergence of crystallinity from fluidized configurations. Because shear melting perturbs initial crystals far from their equilibrium configuration, assembly of new crystalline domains requires extensive particle rearrangements on length scales greater than the particle radii, which corresponds to a long-time self-diffusion process.[6] Because the long-time self-diffusion coefficient and particle diffusion rate, λ_{diff}, decrease with

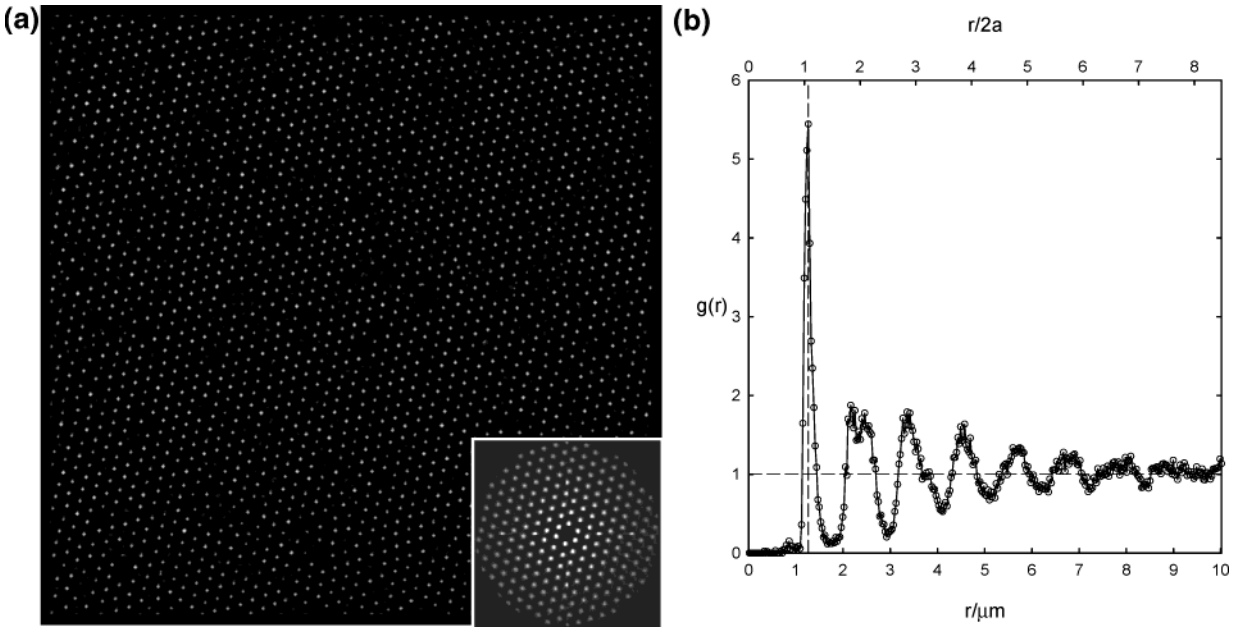

Figure 6. (a) Reflectance image and two-dimensional number density, $N(r,\theta)$ (inset), for the first layer of colloidal crystal observed at completion of the multiple step electrolyte diffusion experiment (see the corresponding kinetic data in Figure 5); (b) radial distribution function, $g(r)$.

diminishing particle separation[38] and particle separation decreases exponentially with increasing ionic strength, the diffusion-limited rate at which particles can rearrange is reduced dramatically with increasing ionic strength. As particles approach contact and experience adhesive interactions, the particle diffusion rate vanishes to zero and particle rearrangement processes become infinitely long. As a direct consequence of the dramatically slowed particle diffusion rates at elevated ionic strengths, the shear-melted configurations in the injection experiments in Figure 3 evolve into less ordered structures with increasing ionic strength. This yields polycrystalline structures at low ionic strengths and irreversible gels at high ionic strengths (see Table 1).

Single step diffusion of electrolyte through membranes was employed to minimize disruption to the initial crystallinity easily generated at low ionic strengths. Despite eliminating forced convection via introduction of a membrane barrier, a trend of diminishing order with increasing ionic strength was observed, similar to the injection experiments (see Table 1). A modest improvement in the degree of order was observed using this approach because initial crystals were perturbed to a lesser extent than in the shear conditions encountered in injection experiments. The observed decrease in order with increasing electrolyte concentration most likely originates from gradient-driven transport effects.[39] Significant electrolyte gradients are expected to arise due to lack of control over the time evolution of electrolyte concentration at the membrane surface above the sedimented crystal (see Figure 1). The magnitude of this gradient depends on the ionic strength difference across the membrane; therefore, the extent of disruptive gradient-driven transport is expected to be significant for large changes in electrolyte concentration. As expected, we observed little disruption to the initial crystallinity at low ionic strengths ($\leq$10 mM NaCl) in the presence of small gradients. However, the larger gradients occurring at higher ionic strengths ($\geq$100 mM NaCl) produced fluidized configurations analogous to those observed upon shear melting. Although single step diffusion disrupted initial crystallinity to a lesser extent than injection to ultimately produce more ordered structures, both methods fail at high ionic strengths because diffusion-limited rearrangements of particles in close proximity inhibit the re-emergence of crystalline configurations.

The multistep diffusion of electrolyte solutions through a dialysis membrane in Figure 5 represents the most highly controlled approach. This method was designed to eliminate forced convection and minimize gradient-driven transport mechanisms that disrupt crystallinity. The electrolyte transport rate was regulated by incrementally increasing the solution ionic strength in the dialysis tube reservoir at selected time intervals. This provided a degree of control over the time evolution of the average electrolyte concentration and gradients in the sedimentation cell not possible with the other approaches. By eliminating deleterious transport effects, single domain, ordered structures were preserved at all ionic strengths (see Table 1) even as individual particles came into adhesive contact (see Figure 6).

Though not reported in the results, a number of separate multistep diffusion experiments were investigated using different electrolyte delivery rates. Those observations revealed the critical influence of the instantaneous structural contraction rate, $\lambda_{contract}$, in determining whether order was retained or not. When electrolyte solutions in the dialysis tube were exchanged frequently to yield fast contraction rates, partially or completely fluidized configurations were observed similar to "single step" diffusion experiments at high ionic strengths (i.e., $\geq$100 mM NaCl in Figure 4c,d). In contrast, exchanging electrolyte solutions less frequently produced slower contraction rates that retained a degree of crystallinity similar within experimental error to the result in Figure 5. These additional multistep diffusion experiments demonstrated that in the absence of disruptive transport effects, the structural contraction rate alone determined whether initial crystallinity was preserved.

To understand the influence of contraction rate on structural evolution in our experiments, it is essential to recognize that the contraction process inherently involves particle rearrangements associated with increasing particle number density. The insertion of added particles into a given layer from above layers necessarily involves many body rearrangements via self-diffusion. To preserve crystallinity as particle separation decreases, the contraction rate must be sufficiently slow to allow particles to rearrange and maintain their lowest free energy configuration throughout the contraction process. Estimates of λ_{diff} and $\lambda_{contract}$ for the multistep diffusion experiment in Figure 5 indicate that the particle diffusion rate exceeds the structural contraction rate by nearly an order of magnitude during most of the contraction process allowing retention of the initial crystalline configuration. As particles approach contact, these rates (and their ratio) cannot be measured because they vanish simultaneously, and confocal scanning laser microscopy does not permit adequate measurement at the relatively small length scales involved. Nevertheless, by carefully regulating electrolyte delivery rate and associated rate of decrease in particle separation, the initial crystallinity in Figure 5 was preserved by allowing the evolving structure to successfully re-equilibrate throughout the entire electrolyte addition and structural contraction process.

Conclusions

We have demonstrated a new assembly route for creating large, mechanically robust, colloidal crystals. Our approach exploits the inherent long-range order of initially low ionic strength colloidal crystals by preserving their structure even as colloidal particles come into adhesive contact in response to controlled, multistep electrolyte diffusion. The importance of both hindered particle diffusion and contraction rates on the structural evolution of colloidal crystals was demonstrated for changing ionic strength via direct injection and single and multistep diffusive transport. With further optimization of these critical parameters, it may be possible to generate colloidal crystals with an even greater degree of perfection than those observed in this investigation.

Acknowledgment. This material is based upon work supported by the Beckman Institute for Advanced Science and Technology at the University of Illinois at Urbana–Champaign (UIUC) and the National Science Foundation (DMR 00-71645). We are grateful to the Imaging Technology Group at the Beckman Institute for the use of their facilities. M.A.B. acknowledges support through the Beckman Fellows program at the Beckman Institute, UIUC.

LA0492658

(38) van Blaaderen, A.; Peetermans, J.; Maret, G.; Dhont, J. K. G. *J. Chem. Phys.* **1992**, *96*, 4591.

(39) Ebel, J. P.; Anderson, J. L.; Prieve, D. C. *Langmuir* **1987**, *4*, 396.